

# Photocatalytic activity of titanium oxide prepared by liquid phase deposition (LPD)

Hirotsugu Kishimoto,<sup>\*†a</sup> Koichi Takahama,<sup>a</sup> Noboru Hashimoto,<sup>a</sup> Yoshifumi Aoi<sup>b</sup> and Shigehito Deki<sup>c</sup>

<sup>a</sup>Matsushita Electric Works, Ltd, 1048 Kadoma, Osaka 571, Japan

<sup>b</sup>Department of Materials Chemistry, Faculty of Science and Technology, Ryukoku University, Seta, Otsu 520–21, Japan

<sup>c</sup>Department of Chemical Science & Engineering, Faculty of Engineering, Kobe University, Rokkodai-cho, Nada, Kobe 657, Japan

Titanium oxide powder and thin films were prepared from an  $(\text{NH}_4)_2\text{TiF}_6$  aqueous solution upon addition of boric acid in a process denoted as liquid phase deposition (LPD). In this process, titanium oxide powder and films were formed by the chemical equilibrium reaction between titanium fluoro-complex ions and metal oxide in the aqueous solution. The prepared powder and deposited films showed some features which differed from titanium oxide prepared from titanium alkoxide. The prepared powder and the deposited films included anatase ( $\text{TiO}_2$ ) and showed photocatalytic activity without prior calcination. The decomposition rate of  $\text{CH}_3\text{CHO}$  reached a maximum when the powder or films were calcined at  $300^\circ\text{C}$ . The LPD process enabled a uniform layer of  $\text{TiO}_2$  film to form homogeneously on the entire surface of glass wool. The prepared  $\text{TiO}_2$  contained fluorine and nitrogen. The amount of these impurities was reduced upon calcination.

## Introduction

In recent years, attention has been directed toward the photocatalytic degradation of organic and inorganic molecules on illuminated surfaces of metal oxide semiconductor powders or thin films such as  $\text{TiO}_2$  and  $\text{ZnO}$ .<sup>1–5</sup> When these semiconductors are illuminated with light of wavelength below 380 nm, excited-state electron and hole pairs are produced, which are capable of initiating a wide variety of chemical reactions.

These metal oxide thin films are usually prepared by dry processes such as CVD, or wet processes such as the sol–gel method. However, these methods have some disadvantages for industrial applications. Other methods using vacuum conditions require expensive equipment and there are still some problems coating large area substrates. Pyrolytic methods restrict the use of substrates because of the high temperatures ( $> 500^\circ\text{C}$ ) required. Recently, a new wet process for preparing metal oxide thin films has been developed<sup>6–8</sup> termed liquid phase deposition (LPD). In this process, metal oxide thin films can be deposited on immersed substrates *via* a chemical equilibrium reaction between a metal fluoro-complex and a metal oxide in aqueous solution. With this process, it is easy to coat substrates of large surface area and/or complex morphologies at room temperature without special equipment.

In this study, the photocatalytic activity for the decomposition of  $\text{CH}_3\text{CHO}$  on  $\text{TiO}_2$  thin films prepared by the LPD process was investigated. The photodegradation was carried out using  $\text{TiO}_2$  thin films deposited on soda lime glass, quartz glass, and glass wool. We also prepared  $\text{TiO}_2$  powder using the same aqueous solution for the deposition of the films and investigated its photocatalytic activity, since this gives information for the photocatalytic activity of the films. We illustrate characteristic features of titanium oxide prepared from  $(\text{NH}_4)_2\text{TiF}_6$ , and compare these with  $\text{TiO}_2$  prepared from titanium alkoxide.

## Experimental

### Liquid phase deposition process

The LPD process is indicated in Fig. 1. Ammonium hexafluorotitanate [ $(\text{NH}_4)_2\text{TiF}_6$ ; Morita Kagaku Kogyo Co. Ltd.] and boric acid ( $\text{H}_3\text{BO}_3$ ; Nacalai Tesque Inc.) were dissolved in distilled water. Various compositions of these solutions were mixed and used as treatment solutions. Soda lime glass, quartz glass, and glass wool (mean diameter,  $23\ \mu\text{m}$ ) were used as substrates. The preparation procedure for thin films was as follows: the substrate was degreased and washed ultrasonically, then immersed in the treatment solution, and vertically suspended. The temperature of the treatment solution was kept

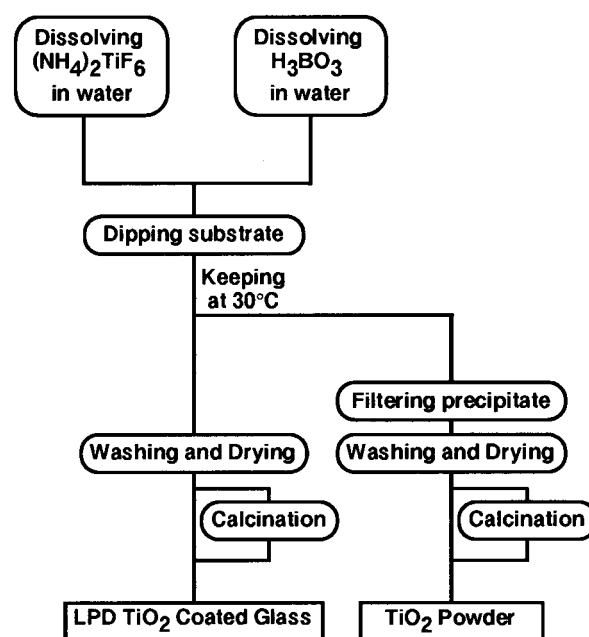


Fig. 1 Schematic diagram of LPD  $\text{TiO}_2$  coating and  $\text{TiO}_2$  powder preparation

<sup>†</sup>E-mail: kishimoto@crl.mew.co.jp

at 30 °C. After a set reaction time, the sample was removed from the treatment solution. It was then washed with distilled water and dried at room temperature. The powders were prepared under the same reaction conditions as the films. After the set reaction time, the precipitate was filtered. It was then washed and dried. Here catalysts were prepared using 0.1 mol dm<sup>-3</sup> (NH<sub>4</sub>)<sub>2</sub>TiF<sub>6</sub> and 0.2 mol dm<sup>-3</sup> H<sub>3</sub>BO<sub>3</sub>, *i.e.* in the concentration range where transparent films can be obtained.<sup>8</sup> Some of these films and powders were calcined at various temperatures.

### Characterization of samples

X-Ray diffraction patterns of the deposited films were measured with a Rigaku RINT 2100 diffractometer using Cu-K $\alpha$  radiation and X-ray diffraction measurements for prepared powders were made with a Rigaku RAD-rX instrument using Cu-K $\alpha$  radiation. UV-VIS spectra were measured with a Shimadzu UV-265FW double-beam digital spectrophotometer. The surface morphology of samples was observed with a scanning electron microscope (SEM; JEOL JSM-5400). The thickness of deposited films, which showed interference patterns, was derived from the visible spectra of the films by the interference method. The BET surface area and pore size distribution of TiO<sub>2</sub> powders were determined by N<sub>2</sub> adsorption using a Quantachrome AUTOSORB-6 set-up. Pore size distributions were estimated by the BJH method.<sup>9</sup> Quantitative analysis of impurities in the prepared powders was carried out as follows: nitrogen was measured by the oxidizing decomposition-vacuum chemiluminescence method, fluorine was measured with an ion selective electrode after dissolving the powder in hydrochloric acid in the presence of sodium carbonate, and boron was measured by inductively coupled plasma atomic emission spectrometry (ICP-AES; Seiko ICP emission spectrometer SPS4000) after dissolving the powder in hydrochloric acid in the presence of sodium carbonate.

### Photocatalytic activity

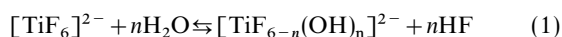
Photodegradation of CH<sub>3</sub>CHO vapour was carried out as follows: 0.1 g of prepared powder, deposited film on planar substrate of area 25 cm<sup>2</sup> or 0.1 g of coated glass wool was placed at the bottom of a quartz glass cell (volume, 300 ml). Then CH<sub>3</sub>CHO was added to the cell to give an initial concentration of 60 ppm. After 60 min, irradiation was commenced. A conventional fluorescent lamp (Matsushita Electric Industry Co., Ltd. Blacklight blue fluorescent tube, 10 W) was used as the light source. The light intensity was 0.65 mW cm<sup>2</sup> at the bottom of the reaction cell as measured by a detector with a wavelength detection range from 320 to 380 nm. The gas in the reaction cell was then removed using a gas syringe at periodic intervals for gas chromatography analysis (Shimadzu GC-14A).

## Results and Discussion

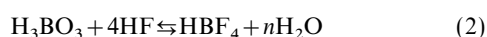
### Deposition and precipitation

After 72 hours of reaction, translucent films were deposited on the substrates and a white powder was simultaneously precipitated.

For the hydrolysis of [TiF<sub>6</sub>]<sup>2-</sup> ions in aqueous solutions, the following equilibrium has been proposed by Schmitt *et al.*<sup>10</sup>



Under the law of mass action, the equilibrium will shift towards the right upon the addition of H<sub>3</sub>BO<sub>3</sub> which acts as an F<sup>-</sup> scavenger. H<sub>3</sub>BO<sub>3</sub> reacts readily with F<sup>-</sup> ions to give the more stable BF<sub>4</sub><sup>-</sup> ion, as follows;<sup>11</sup>



The addition of H<sub>3</sub>BO<sub>3</sub> promotes the consumption of non-coordinated F<sup>-</sup> ions and thus the hydrolysis reaction. From the results of X-ray diffraction, which showed that the deposited film and prepared powder included anatase TiO<sub>2</sub>, it is supposed that the deposition of TiO<sub>2</sub> thin film and precipitation of TiO<sub>2</sub> arose through the dehydration reaction of [TiF<sub>6-n</sub>(OH)<sub>n</sub>]<sup>2-</sup> which was generated by the hydrolysis of [TiF<sub>6</sub>]<sup>2-</sup>. It was reported that SiO<sub>2</sub> films deposited by the LPD process are richer in Si-O-Si bonds compared to other SiO<sub>2</sub> films, and the LPD SiO<sub>2</sub> film has more ordered silica networks.<sup>6</sup> This report and our result of TiO<sub>2</sub> crystal formation imply that the dehydration reaction and the consequent formation of ordered metal-oxygen networks (crystallization) can occur readily in the LPD process.

### TiO<sub>2</sub> powder

Fig. 2 shows X-ray diffraction patterns for a synthesized powder as well as for powders calcined at various temperatures. The powder prior to calcination showed peaks assignable to anatase, and the peak intensity increased with increasing calcination temperature. For samples calcined below 800 °C, diffraction peaks other than that of anatase TiO<sub>2</sub> were not observed. By contrast, it was reported that titanium oxide powder prepared by hydrolysis of titanium alkoxide is amorphous<sup>12</sup> and contains some rutile upon calcination above 600 °C.<sup>13</sup>

The crystallite sizes obtained on the basis of Scherrer's equation for the (101) peak of anatase are indicated in Fig. 3. The crystallite size increased from 3 nm for the as-prepared

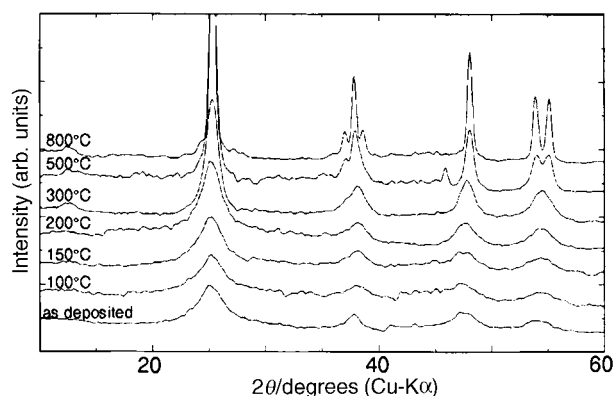


Fig. 2 XRD patterns of the prepared titanium oxide powders. The powders were prepared with 0.1 mol dm<sup>-3</sup> (NH<sub>4</sub>)<sub>2</sub>TiF<sub>6</sub> and 0.2 mol dm<sup>-3</sup> H<sub>3</sub>BO<sub>3</sub> and calcined at various temperatures

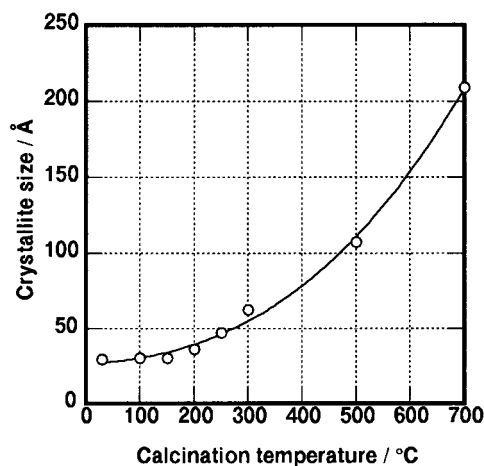


Fig. 3 Effect of calcination temperature on crystallite size of anatase TiO<sub>2</sub> in prepared titanium oxide powders. The crystallite size was obtained by basis of Scherrer's equation for the (101) peak from anatase

powder to *ca.* 20 nm for the powder calcined at 700 °C. As shown in Fig. 4, the crystal content of anatase in the as-prepared powder estimated assuming pure anatase TiO<sub>2</sub> (Merck) was 37% and reached *ca.* 100% when the powder was calcined at 500 °C.

The photocatalytic activities of TiO<sub>2</sub> powder calcined at various temperatures are shown in Fig. 5. The decomposition rate was defined in terms of the half-life of CH<sub>3</sub>CHO. The relationship between the decomposition rate and calcination temperature is shown in Fig. 6. The differences of initial concentration among the profiles in Fig. 5 are due to the adsorption of CH<sub>3</sub>CHO on the powder during the gas syringe manipulations. The TiO<sub>2</sub> powder sample prepared here showed photocatalytic activity even without calcination while the decomposition rate of CH<sub>3</sub>CHO reached a maximum when the powder was calcined at 300 °C; by contrast, titanium oxide prepared from titanium alkoxide generally shows high photocatalytic activity only when calcined at 600–800 °C.<sup>13</sup> The difference is due to the chemical state of the calcined TiO<sub>2</sub> powder, such as the crystallite size, crystal content, specific surface area, impurities, *etc.*

The decomposition rate of CH<sub>3</sub>CHO increased with calcination temperature from 100 to 300 °C, passed through a maximum, and then decreased at temperatures above 300 °C, despite the crystallinity increasing with calcination temperature. In order to understand the decomposition process in detail, the surface morphology of the powder was also

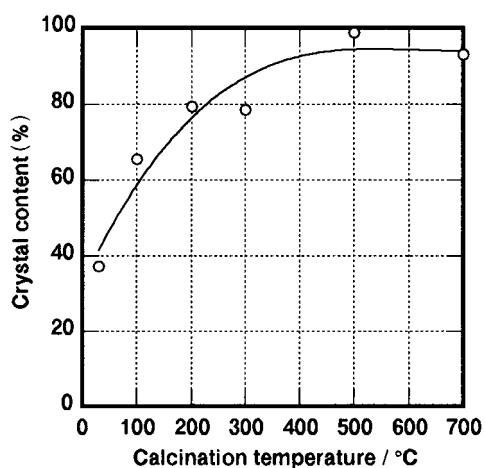


Fig. 4 Effect of calcination temperature on crystal content of anatase TiO<sub>2</sub> in prepared titanium oxide powder. The crystal content of anatase in the powders was estimated using pure anatase TiO<sub>2</sub>.

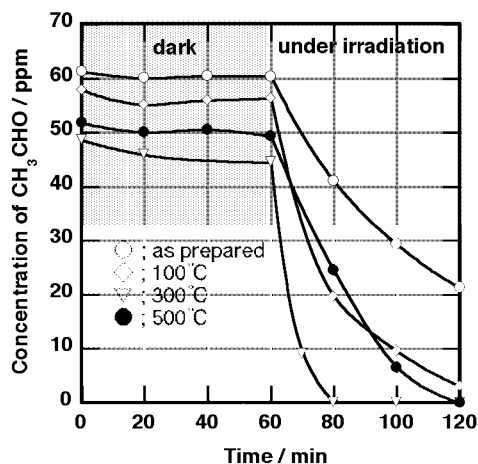


Fig. 5 Reaction profiles of the photocatalytic decomposition of CH<sub>3</sub>CHO on TiO<sub>2</sub> powder. The powders were prepared with 0.1 mol dm<sup>-3</sup> (NH<sub>4</sub>)<sub>2</sub>TiF<sub>6</sub> and 0.2 mol dm<sup>-3</sup> H<sub>3</sub>BO<sub>3</sub>. The powders were: (○) as prepared, (◇) calcined at 100, (▽) 300 and (●) 500 °C.

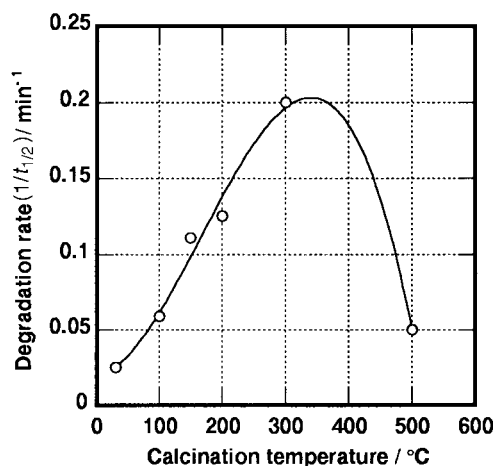


Fig. 6 Effect of calcination temperature on photocatalytic decomposition rate of CH<sub>3</sub>CHO on TiO<sub>2</sub> powder. The decomposition rate was defined in terms of the half life of CH<sub>3</sub>CHO.

investigated as a factor, which affects photocatalytic activity as well as the crystallinity of anatase TiO<sub>2</sub>.

The relationship between the specific surface area of the prepared powder and calcination temperature is shown in Fig. 7. The specific surface area increased with calcination temperature, passed through a maximum, and then decreased at temperatures above 300 °C with the profile being similar to the reactivity profile of Fig. 6.

Pore size distributions and total pore volume of the powder calcined at various temperatures are shown in Fig. 8 and 9, respectively. Titanium oxide powder, heated below 100 °C, showed pores with radii < 20 Å. Pores of radius from 20 to 80 Å were formed upon calcination at 300 °C. This was because the amorphous phase in the titanium oxide powder transformed into higher density anatase. This pore formation leads to an increase of the total pore volume and specific surface area. On the other hand, in the sample calcined at 500 °C, the number of pores below 80 Å decreased owing to crystal growth, and therefore the total pore volume and specific surface area decreased.

It appears that the large specific surface area and high crystallinity of anatase TiO<sub>2</sub> contributes to the high decomposition rate of TiO<sub>2</sub> powder calcined at 300 °C, whereas for the sample calcined at 500 °C, the decomposition rate became lower owing to the decrease of specific surface area as a consequence of crystal growth.

The relationship between the specific decomposition rate per unit surface area of the catalyst and calcination temperature is shown in Fig. 10. When the powder was calcined at temperatures

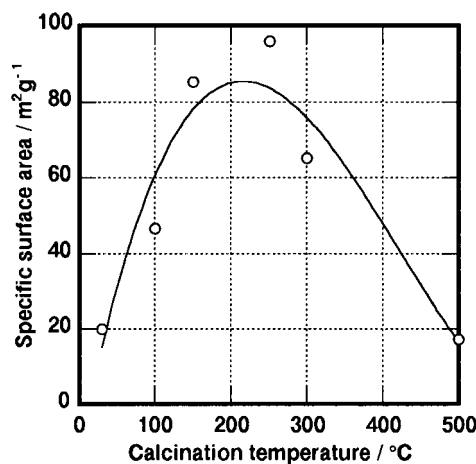


Fig. 7 Effect of calcination temperature on the specific surface area of prepared titanium oxide powders

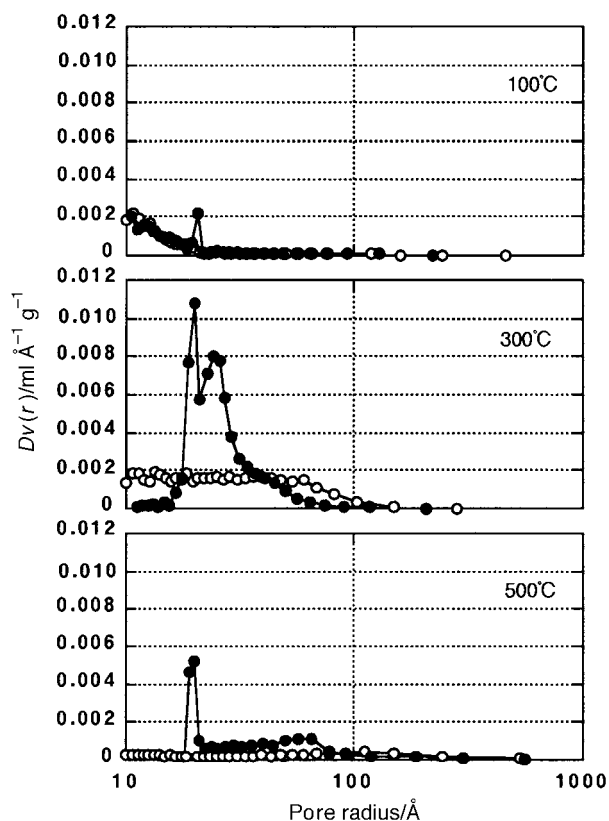


Fig. 8 Pore size distributions of titanium oxide powders calcined at various temperatures. Pore size distributions were estimated by the BJH method<sup>9</sup> using: (○) adsorption curves and (●) desorption curves

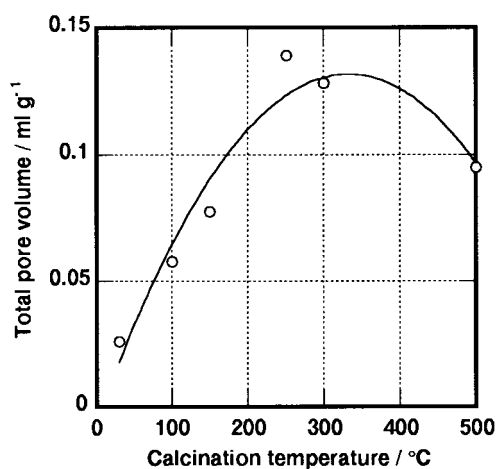


Fig. 9 Effect of calcination temperature on total pore volume of titanium oxide powders

between 150 and 300 °C, the specific decomposition rate increased. X-Ray diffraction data suggest that amorphous phase transformed into anatase in this temperature range. The specific decomposition rate did not vary with calcination at temperatures between 300 °C and 500 °C. This suggests that sintering of anatase TiO<sub>2</sub> particles and crystal growth occurred above 300 °C.

#### Films on sheet glass substrates

X-Ray diffraction measurements for deposited films showed that they consisted of anatase TiO<sub>2</sub> and titanium oxide in the amorphous phase as for the powder. The crystallite size calculated by Scherrer's equation for the (101) peak of anatase was several nanometers for the as-deposited film and ca. 20 nm for the film calcined at 600 °C for which no diffraction peaks other than those of anatase TiO<sub>2</sub> were observed.

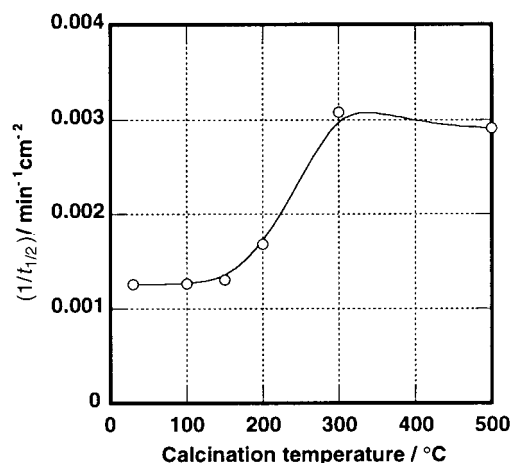


Fig. 10 Effect of calcination temperature on photocatalytic activity of titanium oxide powders. The photocatalytic activity was determined as the specific decomposition rate per unit surface area of the titanium oxide powder.

The decomposition rate of CH<sub>3</sub>CHO on the deposited film was also a maximum when the film was calcined at 300 °C. The thickness of each film was ca. 950 nm. The effect of the film thickness on the photocatalytic activity was investigated. Similar to a previous report,<sup>14</sup> the photocatalytic activity increased with increase of film thickness up to 700 nm, and showed a constant value above 700 nm. Fig. 11 shows the decomposition of CH<sub>3</sub>CHO on films on soda lime glass and on quartz glass. Both films were calcined at 300 °C and exhibited the same decomposition rate. These results suggest that the migration of alkali metal ions from soda lime glass of the substrate did not occur upon calcination at 300 °C, and the photocatalytic activity for the film calcined at 300 °C was not affected by the nature of the substrates.

Fig. 12 shows AFM micrographs of films calcined at various temperatures. Films were deposited very uniformly and showed uniform interference color. On the other hand, AFM observations showed that the film consisted of the fine particles below 50 nm in diameter and some large particles of > 500 nm (Fig. 12A). It is considered that the large particles formed from the bulk of the solution. When the film was calcined at 300 °C, the roughness of the surface did not alter from the as-deposited film (Fig. 12B) but the crystallinity increased. This film exhibited high photocatalytic activity for the decomposition of CH<sub>3</sub>CHO. The surface morphology of the film calcined at 500 °C became smooth (Fig. 12C) and is the reason why the

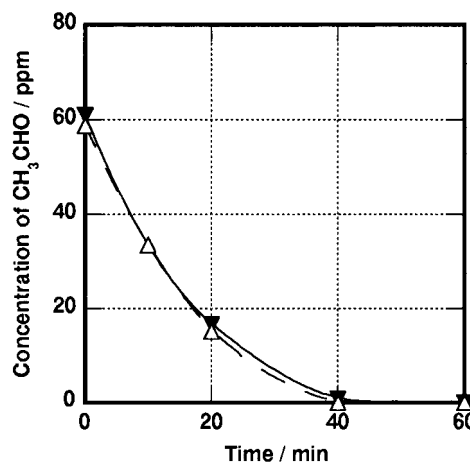


Fig. 11 Effect of substrates on the photocatalytic decomposition of CH<sub>3</sub>CHO on the TiO<sub>2</sub> films calcined at 300 °C. The films were deposited on (▼) soda lime glass and (△) quartz glass with 0.1 mol dm<sup>-3</sup> (NH<sub>4</sub>)<sub>2</sub>TiF<sub>6</sub> and 0.2 mol dm<sup>-3</sup> H<sub>3</sub>BO<sub>3</sub>.

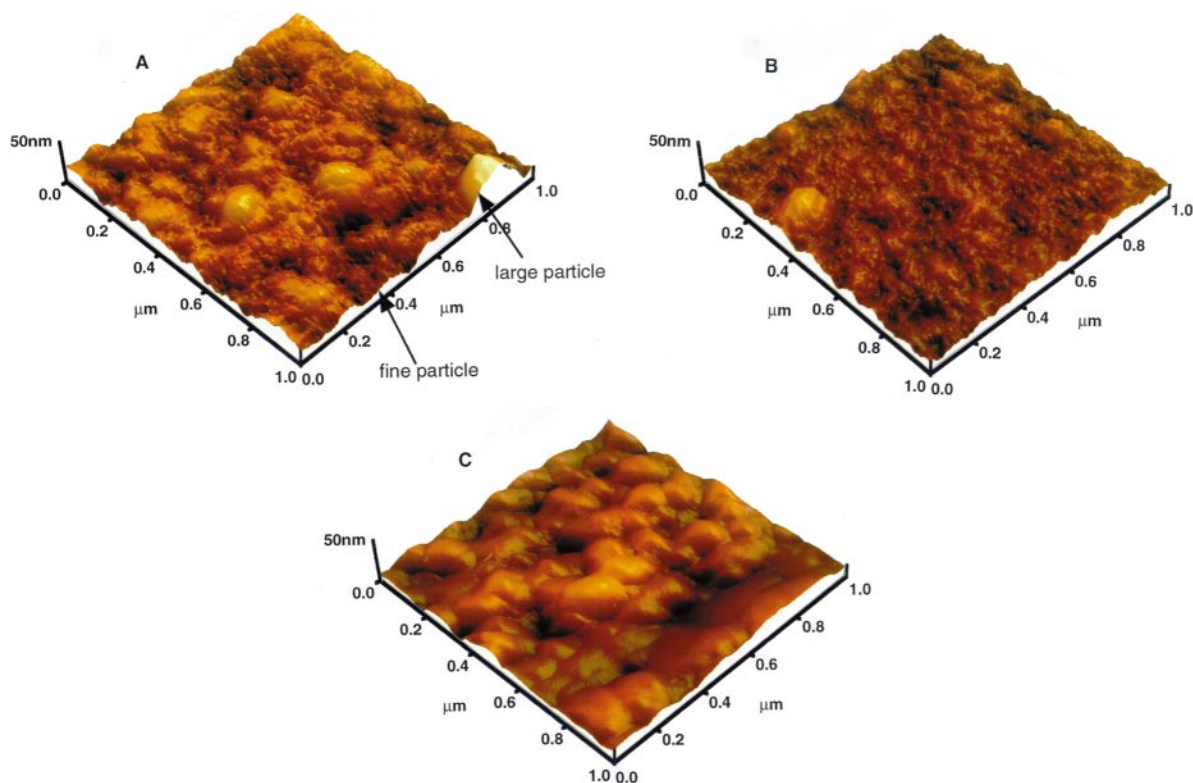


Fig. 12 AFM photographs of deposited films on soda lime glass: (A) as prepared, (B) calcined at 300 °C and (C) calcined at 500 °C

photocatalytic activity decreased, even though the crystallinity of anatase TiO<sub>2</sub> increased. These phenomena mirrored the photocatalytic activity of the powder.

#### Film on glass wool

Photocatalysts on substrates with complex morphologies and large specific surface areas, such as glass wool, are useful for the decomposition of organic impurities in air or water.<sup>15–22</sup> However, it is difficult to prepare TiO<sub>2</sub> films uniformly over the entire surface of glass wool or to bind TiO<sub>2</sub> powder on it *via* ordinary methods. On the other hand, the LPD process is suitable for forming uniform TiO<sub>2</sub> films on substrates with complex surfaces such as glass wool.

SEM micrographs of films deposited on glass wool and of the glass wool substrate are shown in Fig. 13A and B, respectively. The film sample was calcined at 300 °C and the TiO<sub>2</sub> film uniformly covered the entire surface of the glass wool as indicated by energy dispersion X-ray analysis (EDX). Some

cracks were observed for the film, owing to the increase of the internal stress with shrinkage of the film by evaporation of water during the drying process.

The photocatalytic activity of films deposited on glass wool prior to calcination is shown in Fig. 14. The film showed photocatalytic activity without post-heat treatment while the decomposition rate of CH<sub>3</sub>CHO showed a maximum value when the powder was calcined at 300 °C. The TiO<sub>2</sub> thin film coated glass wool calcined at 300 °C has such a high photocatalytic activity that it could decompose CH<sub>3</sub>CHO using an ordinary fluorescent lamp (10 W) as indicated in Fig. 15. The light intensity was 0.01 mW cm<sup>-2</sup> as measured by a detector with a wavelength detection range from 320 to 380 nm.

#### Crystal formation and transformation of LPD-TiO<sub>2</sub>

Titanium oxide synthesized by the hydrolysis of titanium alkoxide is amorphous.<sup>12</sup> On the other hand, the powder prepared from (NH<sub>4</sub>)<sub>2</sub>TiF<sub>6</sub> in this study contained anatase

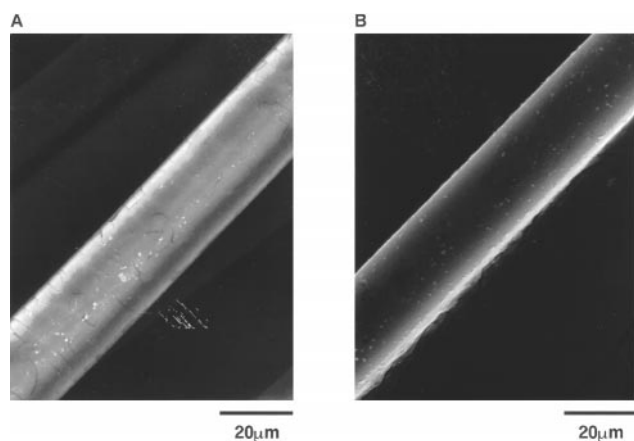


Fig. 13 (A) SEM photograph of the film deposited on glass wool with 0.1 mol dm<sup>-3</sup> (NH<sub>4</sub>)<sub>2</sub>TiF<sub>6</sub> and 0.2 mol dm<sup>-3</sup> H<sub>3</sub>BO<sub>3</sub>. (B) SEM photograph of glass wool used as the substrate.

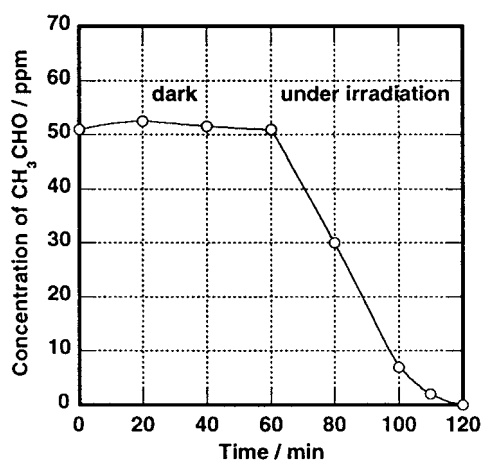
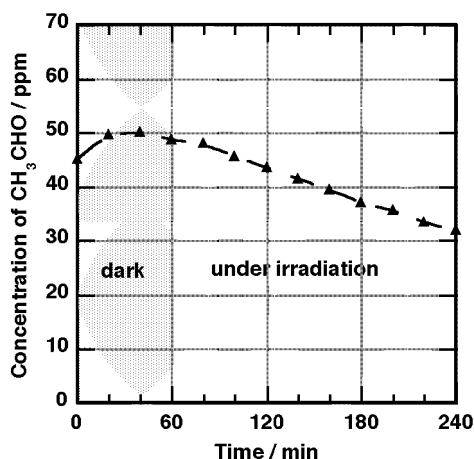


Fig. 14 Reaction profile of the photocatalytic decomposition of CH<sub>3</sub>CHO on the as-deposited titanium oxide film on glass wool



**Fig. 15** Reaction profile of the photocatalytic decomposition of CH<sub>3</sub>CHO on TiO<sub>2</sub> film on glass wool under illumination (10 W fluorescent lamp). The films were: (○) as deposited and (▲) calcined at 300 °C.

TiO<sub>2</sub>, which is similar to the titanium oxide powder prepared from thermal hydrolysis of a titanium oxysulfate aqueous solution.<sup>23,24</sup> The difference may possibly derive from the difference between the shapes of the solute species or complexes such as TiF<sub>6</sub><sup>2-</sup> and Ti(OR)<sub>4</sub>. The shape of TiF<sub>6</sub><sup>2-</sup> in an aqueous solution of (NH<sub>4</sub>)<sub>2</sub>TiF<sub>6</sub> is octahedral,<sup>25,26</sup> which may lead to TiO<sub>6</sub> octahedra consisting of anatase. In the hydrothermal hydrolysis process, mononuclear fluoro complexes of titanium are unstable towards hydrolysis at high supersaturation, and polymerize to afford polynuclear complexes (embryos) related structurally to anatase; further polymerization leads to the nucleation of anatase, which is followed by the growth of the resulting crystal nuclei.<sup>27</sup> The reason for the formation of anatase TiO<sub>2</sub> in the LPD process has not been determined, but it may be *via* polynuclear fluoro complexes with edge-shared skewed octahedra.

It is also well known that TiO<sub>2</sub> particles prepared from titanium alkoxide and calcined at >600 °C contain some rutile.<sup>13</sup> However, the TiO<sub>2</sub> powder prepared from ammonium hexafluorotitanate aqueous solution in this study did not. It is also known that transformation from anatase to the more thermodynamically stable rutile is inhibited by the addition of strongly titanium complexing ions, such as sulfate, phosphate or fluoride.<sup>26–33</sup> This is because the ligand prevents the condensation of TiO<sub>6</sub> octahedra by opposite edges to form linear chains of rutile, while growth of spiral chains of TiO<sub>6</sub> octahedra characteristic of anatase is still possible.<sup>31</sup>

Table 1 shows the results of analysis of impurities of the prepared powder calcined at various temperatures. The results indicate that the prepared powder scarcely contains boron (<0.001 wt.%). Nitrogen from ammonium ions could be burned off, however, fluoride ion was not burned off even at 500 °C. Thus titanium oxide prepared from (NH<sub>4</sub>)<sub>2</sub>TiF<sub>6</sub> did not transform into rutile even upon calcination at 800 °C since fluoride ion is incorporated into the anatase lattice, which may substitute for oxygen in TiO<sub>2</sub> and act as a donor dopant. We will report in the future on the effect of fluoride ion on crystal formation and photocatalytic activity.

**Table 1** Amount of impurities in TiO<sub>2</sub> powder calcined at various temperatures

	F (mass %)	B (mass %)	N (mass %)
as prepared	7.2	<0.001	1.520
300 °C	4.6	<0.001	0.920
500 °C	0.63	<0.001	0.021

## Conclusion

We were able to prepare TiO<sub>2</sub> (anatase) powder and films *via* a new synthesis method using the chemical equilibrium reaction in (NH<sub>4</sub>)<sub>2</sub>TiF<sub>6</sub> solution. The following can be concluded.

1. The powder and film showed photocatalytic activity prior to calcination.
2. The decomposition rate of CH<sub>3</sub>CHO was highest when the powder was calcined at 300 °C.
3. The photocatalytic activity of the film calcined at 300 °C was not affected by the nature of the substrate.

We were also able to prepare TiO<sub>2</sub> (anatase) thin films uniformly on glass wool. It is concluded that the fibrous material which is coated with TiO<sub>2</sub> using the LPD process is effective for the photocatalytic decomposition of organic materials in gaseous or liquid states without pre-coating.

## References

- 1 N. B. Jacson, C. M. Wang, Z. Luo, J. Schwitzgebel, J. G. Ekerdt, J. R. Brock and A. Heller, *J. Electrochem. Soc.*, 1991, **138**, 3660.
- 2 H. Yoneyama, Y. Yamashita and H. Tamura, *Nature (London)*, 1979, **282**, 817.
- 3 M. Abdullah, G. K. C. Low and R. W. Matthews, *J. Phys. Chem.*, 1990, **94**, 6280.
- 4 D. Bahnmann, J. Cunningham, M. A. Fox, E. Pelizzetti, P. Pichat and N. Serpone, in *Aquatic and Surface Photochemistry*, ed. G. R. Helz, R. G. Zepp and D. G. Crosby, Lewis, Boca Raton, FL, 1994, pp. 261–316.
- 5 P. Pichat, in *Handbook of Heterogeneous Catalysts*, ed. G. Ertl, H. Knöinger and J. Weitkamp, VCH-Wiley, New York, 1997, vol. 4, pp. 2111–2122.
- 6 H. Nagayama, H. Honda and H. Kawahara, *J. Electrochem. Soc.*, 1988, **135**, 2013.
- 7 A. Hishinuma, T. Goda, M. Kitaoka, S. Hayashi and H. Kawahara, *Appl. Surf. Sci.*, 1991, **48/49**, 405.
- 8 S. Deki, Y. Aoi, O. Hiroi and A. Kajinami, *Chem. Lett.*, 1996, **6**, 433.
- 9 E. P. Barrett, L. G. Joyner and P. P. Halenda, *J. Am. Chem. Soc.*, 1951, **73**, 373.
- 10 R. H. Schmitt, E. L. Glove and R. D. Brown, *J. Am. Chem. Soc.*, 1960, **82**, 5292.
- 11 C. A. Wamser, *J. Am. Chem. Soc.*, 1951, **73**, 409.
- 12 I. Manzini, G. Antonioli, D. Bersani, P. P. Lottici and A. Montenero, *J. Non-Cryst. Solids*, 1995, **192**, 519.
- 13 K. Kato, *Bull. Chem. Soc. Jpn.* 1992, **65**, 34.
- 14 H. Cui, H-S. Shen, Y-M. Gao, K. Dwight and A. Wold, *Mater. Res. Bull.*, 1993, **28**, 195.
- 15 K. Kato, *J. Ceram. Soc. Jpn.*, 1993, **101**, 245.
- 16 M. Anpo, N. Aikawa, Y. Kubokawa, M. Che, C. Louis and E. Giamello, *J. Phys. Chem.*, 1985, **89**, 5017.
- 17 K. Domen, Y. Sakata, A. Kudo, K. Maruya and K. Onishi, *Bull. Chem. Soc. Jpn.*, 1988, **61**, 359.
- 18 M. Takahashi, K. Mita, H. Toyuki and M. Kume, *J. Mater. Sci.*, 1989, **24**, 243.
- 19 T. Hisanaga and K. Tanaka, *Denki Kagaku*, 1992, **60**, 107.
- 20 R. W. Matthews, *Sol. Energy*, 1987, **38**, 405.
- 21 R. W. Matthews, *J. Phys. Chem.*, 1987, **91**, 3228.
- 22 H. Al-Ekabi and N. Serpone, *J. Phys. Chem.*, 1988, **92**, 5276.
- 23 S. Nishimoto, B. Ohtani, A. Sakamoto and T. Kagitani, *J. Chem. Soc. Jpn.*, 1984, **2**, 246.
- 24 A. Kurosaki and S. Okazaki, *J. Chem. Soc. Jpn.*, 1976, 1816.
- 25 P. A. Dean and D. F. Evans, *J. Chem. Soc. A*, 1967, 698.
- 26 V. P. Tarasov and Y. A. Buslaev, *J. Magn. Reson.*, 1977, **25**, 197.
- 27 F. Izumi and Y. Fujiki, *Bull. Chem. Soc. Jpn.*, 1976, **49**, 709.
- 28 L. I. Bekkerman, I. P. Dobrovol'skii and A. A. Ivakin, *Russ. J. Inorg. Chem.*, 1976, **21**, 223.
- 29 V. A. Kuznetsov, *J. Cryst. Growth*, 1968, **3/4**, 405.
- 30 M. Passaret, Y. Tondic, A. Regreny, R. Aumont and J. F. Bayon, *J. Cryst. Growth*, 1972, **13/14**, 524.
- 31 F. Izumi, *Bull. Chem. Soc. Jpn.*, 1978, **51**, 1771.
- 32 E. Narita, H. Takeuchi, N. Horiguchi and T. Okabe, *Bull. Chem. Soc. Jpn.*, 1984, **57**, 1388.
- 33 T. R. N. Kutty, R. Vivekanandan and P. Murugaraj, *Mater. Chem. Phys.*, 1988, **19**, 533.